THE JOURNAL OF PHYSICAL CHEMISTRY A

Article

pubs.acs.org/JPCA

Hot Band Spectroscopy of the Formyl Cation, $H^{12}C^{16}O^+$

Christopher F. Neese,*[,†,∥] Peter S. Kreynin,[‡] and Takeshi Oka*[,†,§]

[†]Department of Chemistry and the Enrico Fermi Institute, University of Chicago, Chicago, Illinois 60637, United States

[‡]Physics, School of Natural Sciences, University of Newcastle upon Tyne, Newcastle upon Tyne NE1 7RU, U.K.

[§]Department of Astronomy & Astrophysics, University of Chicago, Chicago, Illinois 60637, United States

Supporting Information

ABSTRACT: Midinfrared spectra of the formyl cation, HCO^+, were recorded by direct absorption in a glow discharge (composition CO, 50 mTorr; H_2, 50 mTorr; He, 7 Torr) using a color center laser spectrometer and velocity modulation with heterodyne detection. The bands measured were 10^00-00^00, 11^10-01^10, 12^00-02^00, 12^20-02^20, 10^01-00^01, 11^11-01^11, 20^00-10^00, and 10^02-00^02. These bands were analyzed and fitted together with all other available rotationally resolved spectra to arrive at a new set of spectroscopic constants for HCO^+. The relative intensities were fit to obtain a rotational temperature, T_{rot} = 434 ± 7 K, and vibrational temperatures for each mode, T_1 = 3300 ± 240 K, T_2 = 841 ± 15 K, and T_3 = 3157 ± 68 K.

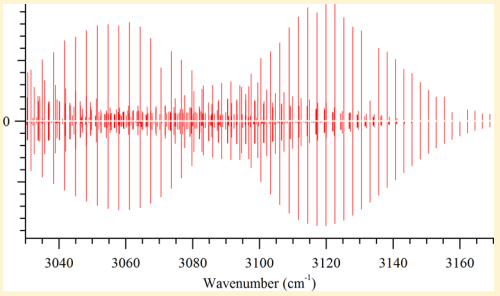

INTRODUCTION

The serendipitous discovery of the millimeter wave X-ogen emission line by Buhl and Snyder in 1970[1] was an epoch-making event for both molecular ion spectroscopy and interstellar chemistry. Klemperer immediately speculated that the carrier of the spectrum was protonated carbon monoxide,[2] and this was confirmed five years later by the laboratory experiment of Woods and colleagues.[3] The HCO^+ line was not only the first rotational line of an ion but was also the first spectrum of a protonated ion in any spectral region. Previously, molecular ion spectroscopy had been limited to electronic spectroscopy of radical ions in the visible and ultraviolet.[4]

HCO^+ was the second molecular ion to be detected in interstellar space after CH^+.[5] Although CH^+ is found in diffuse clouds where the penetrating stellar radiation ionizes atoms and molecules, HCO^+ is mostly found in dense molecular clouds where such radiation is almost completely shielded. The only ionizing agent is the high-energy cosmic rays that penetrate such clouds. Thus the observed high abundance of HCO^+ and the realization that dense clouds are also in the state of weakly ionized plasmas were crucial in advancing the new idea by Herbst and Klemperer[6] and Watson[7] that ion−neutral reactions initiated by cosmic ray ionization was the major mechanism for producing molecules efficiently in the hostile environment of interstellar space with low temperature and density.

This development stimulated laboratory studies of molecular ions in various fields. Many new spectra of molecular ions were uncovered in the infrared and microwave including about 30 protonated ions such as H_3^+, HeH^+, H_3O^+, NH_4^+, HN_2^+, $HCNH^+$, etc.,[8] all very fundamental molecular ions well-known in mass spectrometry but completely unknown spectroscopically. All of them except HeH^+ are abundant in molecular clouds. Rate constants for many ion−neutral reactions were measured,[9] and dissociative recombination of many molecular ions was studied.[10] The development also stimulated ab initio theory of molecular ions.

Because of the special importance of HCO^+, its spectrum has been studied extensively. Many measurements of rotational spectra, in the ground state,[3,11−16] as well as in vibrationally excited states,[16−19] and infrared vibration−rotation spectra[20−26] of $H^{12}C^{16}O^+$ have been reported. The absolute infrared band intensity of the ν_1 fundamental has been measured by direct laser absorption spectroscopy of a fast ion beam.[27] The photoionization spectra of the formyl radical, HCO, provide useful information on highly excited states of the ν_2 mode of HCO^+, as there is a bent to linear geometry change upon ionization.[28−34]

There are also extensive measurements of different isotopologues of the formyl cation. The rotational spectra of the $H^{13}C^{16}O^+$, $H^{12}C^{18}O^+$, $D^{12}C^{16}O^+$, $D^{13}C^{16}O^+$, and $D^{13}C^{18}O^+$ isotopologues were reported shortly after the normal isotopologue[11,13] and were used to calculate the molecular structure of the cation.[13] The $D^{12}C^{16}O^+$ isotopologue has been studied by microwave, infrared, and photoelectron spectroscopies.[11−13,17,28,35−39] The rotational spectrum of the $H^{12}C^{17}O^+$ isotopologue has also been measured.[40−44] The $H^{13}C^{16}O^+$, $D^{12}C^{16}O^+$, $H^{12}C^{18}O^+$, and $H^{12}C^{17}O^+$ isotopologues (as well as $H^{12}C^{16}O^+$) were identified via radioastronomy prior to laboratory spectroscopy.[45,46] Brown has provided a critical compilation of published rotational spectra and molecular constants for isotopologues of HCO^+ up to the year 1995.[47]

Special Issue: Oka Festschrift: Celebrating 45 Years of Astrochemistry

Received: December 31, 2012
Revised: March 13, 2013
Published: March 14, 2013

   dx.doi.org/10.1021/jp312879f | J. Phys. Chem. A 2013, 117, 9899−9907

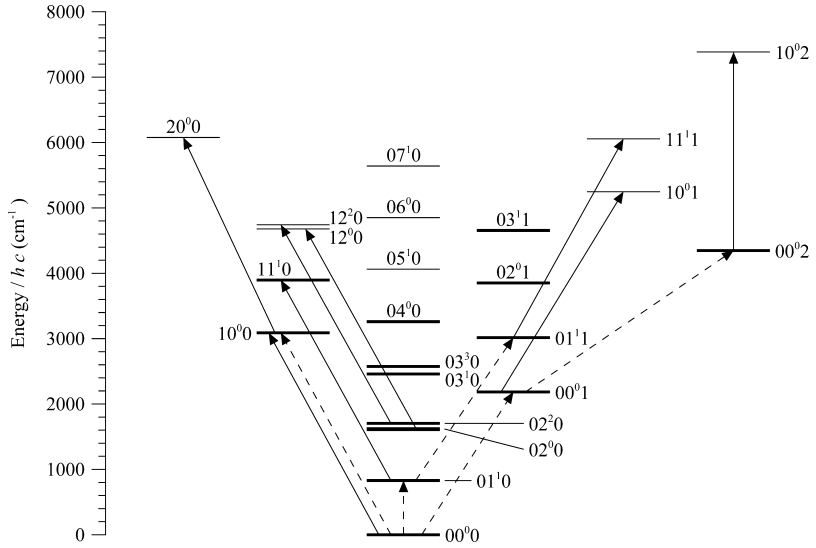

Figure 1. A summary of all measured rotationally resolved transitions of $H^{12}C^{16}O^+$. Thick rules denote vibrational states with measured rotational spectra. Dashed arrows indicate previously measured bands; solid arrows indicate bands measured (or remeasured) in this work. The *l*-type splitting within the 020, 030, and 120 vibrational levels has been greatly exaggerated for clarity.

Guelachvili and Rao have provided a similar compilation of infrared data.[48]

In spite of the extensive studies of HCO^+, there has been measurement of only two infrared hot bands.[26] In this work we present measurements of seven previously unobserved hot bands, 11^10-01^10, 12^00-02^00, 12^20-02^20, 10^01-00^01, 20^00-10^00, 11^11-01^11, and 10^02-00^02, in addition to measurements of the ν_1 fundamental band. The assigned lines were combined with all the known rotationally resolved data available in the literature in a global simultaneous least-squares analysis. The resulting molecular parameters are discussed. A summary of all the known rotationally resolved transitions of $H^{12}C^{16}O^+$ is given in Figure 1.

EXPERIMENTAL METHODS

HCO^+ was generated in a water cooled positive column plasma discharge tube and detected using a color center laser spectrometer that combines velocity modulation[20] and frequency modulation[49] to achieve sensitivity near the shot-noise limit. High sensitivity is a critical aspect of any spectrometer used to study molecular ions, as the fractional ionization of a laboratory plasma is ∼1 ppm. This double modulation technique was developed independently by Long-sheng Ma and others at East China Normal University and was used in combination with magnetic rotation to record the visible spectra of paramagnetic ions.[50,51] We have used this double modulation technique previously to study the visible spectrum of C_2^+,[52] the near-infrared spectra of H_3^+[53] and CH_2^+,[54] and the infrared spectra of $HCNH^+$.

Color Center Laser. The color center laser (FCL) used for this work was a standing wave Burleigh FCL-20 operated with a RbCl:Li-FA(II) crystal that tuned between 3000 and 3700 cm^{-1}. The laser was operated in single mode and pumped with about 1 W from a krypton ion laser (Spectra Physics 171) passed through an acousto-optic power stabilizer (LiCONiX 50SA). The laser is computer automated as described in our previous paper,[55] although for this work the intracavity etalon (ICE) was actively locked to the cavity with custom analog circuitry. The spectrometer can scan in high-resolution over many wavenumbers at tuning rates exceeding 10 cm^{-1}/h.

The spectra recorded by this system are not inherently linear in frequency. In particular, there are small frequency hops associated with racheting the cavity which require correction. We linearize our spectra after data acquisition as part of the data analysis. The linearization algorithm requires a relative frequency measurement that can be either the voltage on the servo-locked ICE or the output of an étalon detector circuit monitoring a 150 MHz spectrum analyzer (Burleigh CFT-500). Our étalon detector circuit is based on the one described by Pate et al.[56] Absolute frequency calibration is done using a reference gas. The output of a Burleigh WA-20 wavemeter is recorded for coarse frequency calibration. For this work the reference gas was ethylene, with line measurements by Pine,[57] which are included in the HITRAN database.[58,59]

Linearization via the ICE provides a frequency precision of approximately 0.003 cm^{-1}, due to the relatively large free spectral range (0.7 cm^{-1}) and low finesse (∼3) of the ICE. The ICE also exhibits some hysteresis, as the scanning rate is not constant. It is relatively easy to correct for this hysteresis, as there are many reference gas lines per ICE mode. Linearization with the 150 MHz spectrum analyzer provides a frequency precision approaching the line width of the laser or spectrum analyzer, approximately 1 MHz. In this case the absolute frequency error is limited by the accuracy of the reference gas measurements, approximately 0.0005 cm^{-1}.

Double Modulation (Velocity Modulation + Frequency Modulation) Technique. The sensitivity of the spectrometer is largely limited by the $1/f$ noise of the laser. To overcome this noise, some combination of modulation, power stabilization, and noise subtraction techniques must be implemented. We use the standard velocity modulation technique,[20] which has recently been reviewed by Stephenson and Saykally.[60] In addition to improving the sensitivity of the spectrometer, selectivity for velocity modulation has the added benefit of a high degree of ion−neutral discrimination.

Velocity modulation alone cannot be done at high enough frequencies to overcome the $1/f$ noise of the color center laser, which does not drop below the fundamental shot-noise limit until about 1 MHz. To further improve the sensitivity, the typical approach has been to use a double beam subtraction

dx.doi.org/10.1021/jp312879f | J. Phys. Chem. A 2013, 117, 9899−9907

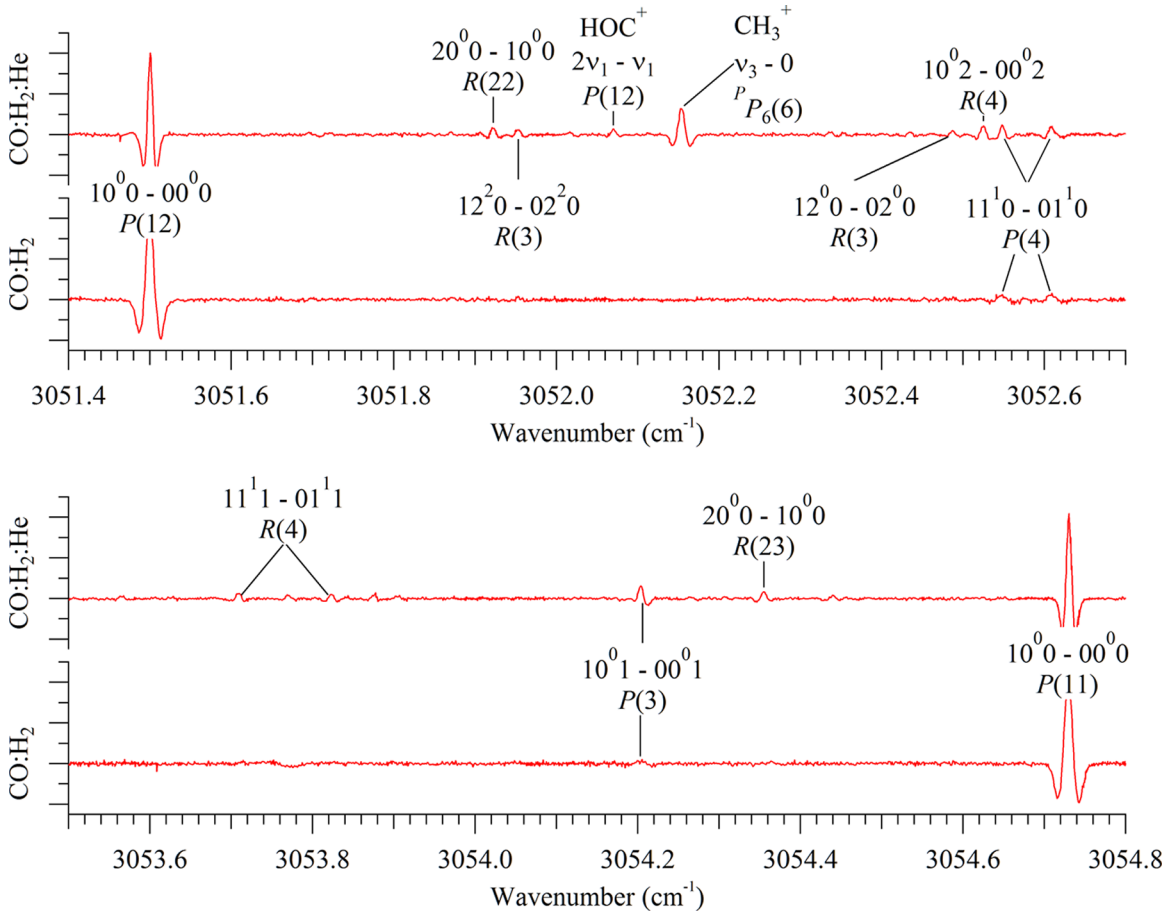

Figure 2. Representative sample of the acquired spectrum of HCO^+, comparing the plasma chemistry with and without He. Lines have a second derivative Gaussian line shape.

method. The most sophisticated version of this scheme from our lab is the autobalanced detection scheme of our previous paper.[55] For this work, we used the frequency modulation technique of Bjorklund,[49] which uses an electro-optic modulator (EOM) to phase modulate the laser at frequencies near the width of a spectral feature. This technique is also known as optical heterodyne detection and is commonly used at visible and near-infrared wavelengths.

The modulation index in this technique is low so that the modulated radiation consists primarily of a carrier and two first-order sidebands. (In practice, higher order sidebands may be significant.) Upon square-law detection, the sidebands beat with the carrier at the modulation frequency, the origin of the optical heterodyne detection moniker. In the absence of a signal, the beat from the negative sideband is 180° out of phase with the beat from the positive sideband. Hence, there is no signal and the $1/f$ laser noise cancels. When the laser is scanned across an absorption feature, the balance between the two sidebands is offset by both the absorption and the dispersion from the spectral feature, and a signal is detected.

The sensitivity of a frequency modulation spectrometer is typically limited by residual amplitude modulation (RAM). RAM destroys the balance of the noise cancelation, and allows $1/f$ noise back into the system, although at a reduced level. Because the level of the $1/f$ noise is decreased, the frequency at which this noise drops below the fundamental shot-noise limit is also decreased. Therefore a second modulation technique, in this case velocity modulation, can reach the shot-noise limit at relatively modest modulation frequencies.

In this experiment, we phase modulated the laser at 77.8 MHz using a 1.5 × 1.5 × 49 mm CdTe EOM. The modulation index was around 1.44 radians, at which point the carrier and first-order sidebands have comparable intensity. The laser was focused through the EOM then recolumnated using two 250 mm CaF_2 lenses. The EOM was aligned to the natural laser polarization of the FCL, so that neither a polarizer nor $\lambda/2$-plate was needed before the EOM. A polarizer was used after the second lens to minimize RAM. After passing through the plasma tube, the laser was focused on a 100 × 100 μm^2 Fast InSb detector (Electro-Optical Systems, Inc.) with a 50 mm CaF_2 lens. The detected RF was mixed down to an IF of 10.7 or 25.0 MHz and then demodulated using a HF lock-in amplifier (Princeton Applied Research PAR100). The velocity modulation signal was then demodulated using a set of lock-in amplifiers.

Positive Column Discharge Cell. The formyl cations, HCO^+, were produced in a water-cooled positive-column discharge tube. The inner bore diameter is 12 mm and the length of the positive column probed by the laser is approximately 1.3 m. The gas mixture is continuously fed to the discharge through 8 inlets and is pumped from the discharge through 5 outlets to a rotary pump. We have used discharge tubes of this design (nicknamed "tarantula") to study a variety of molecular ions.[61] The laser beam was passed 4 times unidirectionally through the tube using a modified White

dx.doi.org/10.1021/jp312879f | J. Phys. Chem. A 2013, 117, 9899−9907

Table 1. Global Fit of HCO^+

Vibrational constants in cm^{-1}					
ω_1	3225.03057(75)		x_{23}	0.01845(69)	
ω_2	843.66539(40)		x_{13}	−26.49913(78)	
ω_3	2217.1632(13)		y_{122}	0.11162(13)	
x_{11}	−49.39681(12)		y_{123}	0.2674(26)	
x_{22}	−2.953		y_{133}	0.31474(19)	
x_{33}	−10.2153(44)		g_e	5.54033(14)	
x_{12}	−24.57268(57)		g_1	−0.146105(78)	
	B_v (MHz)	D_v (kHz)		B_v (MHz)	D_v (kHz)
00^00	44594.42838(57)	82.8202(44)	02^01	44456.6315(49)	86.673(66)
01^10	44677.15056(77)	84.4855(49)	02^21	44430.1149(90)	34.894(102)
02^00	44767.97746(81)	86.5835(64)	11^10	44339.58458(184)	83.8428(143)
02^20	44751.51979(294)	85.8759(200)	00^02	44004.08576(260)	82.9387(190)
01^11	44299.86667(55)	82.9346(39)	03^11	44506.3688(32)	112.490(70)
03^10	44851.41619(186)	88.4545(153)	03^31	44534.44581(265)	214.645(73)
03^30	44817.5739(39)	86.991(32)	12^00	44450.278(214)	88.05(139)
00^01	44374.62998(104)	84.4922(77)	12^20	44455.243(176)	86.58(99)
10^00	44240.53309(56)	82.0927(75)	10^01	43964.872(70)	82.249(184)
04^00	44944.15528(240)	90.4397(172)	11^11	44040.190(106)	87.36(48)
04^20	44926.81105(165)	89.4925(125)	20^00	43925.569(40)	79.427(46)
04^40	44874.64245(185)	88.5222(161)	10^02	43688.821(96)	81.615(250)
	q_v (MHz)	q_{Jv} (kHz)		q_v (MHz)	q_{Jv} (kHz)
010	211.76385(155)	−1.7317(98)	021	226.148(59)	−0.04(70)
020	214.16805[a]	−1.8643[a]	110	203.0754(37)	−1.9665(286)
011	216.57226(189)	−1.9968(153)	031	190.8419(34)	−0.053868(72)
030	223.37420(209)	−1.6699(153)	120	202.77(106)	−6.5(39)
040	220.8256(122)	−1.175(100)	111	262.810(126)	−1.01(79)

[a]The values of q_v and q_{Jv} for the 020 state are interpolated from the 010 and 030 states.

cell, giving a total path length of around 5.2 m. The gas mixture used was 50 mTorr CO, 50 mTorr H_2, and 7 Torr He. The addition of He to the discharge helps to populate the excited vibrational levels that were measured in this work (see, for example, ref 62). We also recorded the spectrum of a 50 mTorr CO, 2 Torr; H_2 discharge for comparison. The discharge current was maintained at around 200 mA and modulated at a frequency of 10 kHz.

RESULTS AND DISCUSSION

Observed Spectrum. A portion of the recorded spectrum, comparing the He-dominated and He-free plasmas, is shown in Figure 2. Our double modulation technique results in a line shape that is very nearly a second derivative of the Doppler-limited Gaussian line shape. The higher vibrational temperatures of the He-dominated plasma are readily apparent in this figure. The lines in the He-dominated plasma are noticeably narrower than in the H_2-dominated plasma. This difference in line width is due to a higher ion drift velocity in the lower pressure H_2-dominated plasma.

In addition to HCO^+, HeH^+, CH_3^+, H_3^+, and $HCNH^+$ were observed in the $He/H_2/CO$ plasma in the region of interest. The $2\nu_1 \leftarrow \nu_1$ band of HOC^+ was observed for the first time in this plasma and will be discussed in a later paper. The spectrum of $HCNH^+$ was very strong in this plasma, even though nitrogen was only present in the plasma as an impurity. Interestingly, the spectrum of HN_2^+ was not observed, indicating that the small N_2 impurity is efficiently converted to HCN.

Line centers and intensities were measured by least-squares fitting of the lines to second-derivative Gaussian functions. The error in the line center from such a fit is normally smaller than the frequency error resulting from linearization and wavelength calibration; hence, the uncertainties that we use to weight our lines in the spectroscopic fitting discussed below are determined by the method of linearization and not the line shape fitting. We do use the error in the intensity from the line shape fitting to relatively weight our temperature fits.

Nomenclature. In this paper, the vibrational levels of HCO^+ are represented by the symbol $v_1v_2^lv_3$. In this notation, v_1, v_2, and v_3 denote the numbers of vibrational quanta in the ν_1 vibrational mode (C−H stretching), the ν_2 vibrational mode (H−C═O bending), and the ν_3 vibrational mode (C═O stretching mode); l is the quantum number associated with the vibrational angular momentum of the doubly degenerate ν_2 bending vibration. Levels with $l > 0$ are doubly degenerate in the rigid-rotor−harmonic-oscillator approximation. These levels are split by l-type doubling and resonance, in which case the two components differ in parity. When such splitting is resolved, the two components are labeled e and f according to the convention of Brown et al.[63]

Hamiltonian Used To Fit the Data. The standard Hamiltonian describing linear molecules has been discussed thoroughly in the literature. The description presented here is based on Winnewisser and Winnewisser[64] and our previous analysis of HN_2^+.[62] It is reproduced here for convenience. The diagonal matrix elements are

$$E = G_v + B_v(J(J+1) - l^2) - D_v(J(J+1) - l^2)^2 \quad (1)$$

where

dx.doi.org/10.1021/jp312879f | J. Phys. Chem. A 2013, 117, 9899−9907

Table 2. Observed Lines of HCO^+ in cm^{-1}

	10^00-00^00		11^10-01^10e		11^10-00^10f		10^01-00^01		020^00-10^00	
	ν	o−c × 10^3	ν	o−c × 10^3	ν	o−c × 10^3	ν	o−c × 10^3	ν	o−c × 10^3
$P(26)$	3003.91968	0.02								
$P(25)$	3007.46216	0.32								
$P(24)$	3010.98242	0.18								
$P(23)$	3014.48047	−0.32								
$P(22)$	3017.95825	0.86								
$P(21)$	3021.41187	−0.11								
$P(20)$	3024.84473	0.25								
$P(19)$	3028.25488	0.08	3004.41626	−0.52	3004.04956	−0.35	3003.24048	−1.00		
$P(18)$	3031.64282	−0.06	3007.77808	−0.26	3007.43579	−0.19	3006.58691	−0.32		
$P(17)$	3035.00855	−0.07	3011.11890	−0.08	3010.80078	0.24	3009.91211	0.21		
$P(16)$	3038.35205	0.08	3014.43872	0.11	3014.14331	−0.20	3013.21484	−0.59		
$P(15)$	3041.67285	0.02	3017.73779	0.64	3017.46582	1.01	3016.49878	1.04		
$P(14)$	3044.97119	0.05	3021.01221	−2.32	3020.76416	−0.21	3019.75879	0.04		
$P(13)$	3048.24683	0.00	3024.27100	0.33	3024.04224	0.12	3022.99902	0.62		
$P(12)$	3051.50000	0.19	3027.50537	−0.13	3027.29834	0.36	3026.21631	−0.29		
$P(11)$	3054.72998	−0.04	3030.71973	0.79	3030.53198	0.11	3029.41333	0.04		
$P(10)$	3057.93750	0.12	3033.91113	0.21	3033.74390	0.17	3032.58862	0.23		
$P(9)$	3061.12183	0.02	3037.08154	0.17	3036.93408	0.60	3035.74170	−0.13		
$P(8)$	3064.28369	0.43	3040.23047	0.26	3040.10132	0.26	3038.87378	0.24		
$P(7)$	3067.42163	−0.02	3043.35718	−0.20	3043.24658	0.20	3041.98364	0.20		
$P(6)$	3070.53882	1.92	3046.46265	−0.15	3046.36987	0.49	3045.07178	0.30		
$P(5)$	3073.62109	−7.86	3049.54614	−0.25	3049.46826	−1.73	3048.13745	−0.12		
$P(4)$	3076.69873	1.01	3052.60864	0.54	3052.54785	−0.28	3051.18189	0.24		
$P(3)$	3079.74048	−2.68	3055.64746	−0.39	3055.60400	0.26	3054.20361	−0.05		
$P(2)$	3082.76538	0.19	3058.66528	−0.30	3058.63721	0.47	3057.20361	0.10		
$P(1)$	3085.76343	−0.31					3060.18115	0.00		
$R(0)$	3091.68823	−1.92					3066.07007	0.55		
$R(1)$	3094.61865	0.78					3068.97852	−1.59		
$R(2)$	3097.51929	−2.57	3073.42334	1.93	3073.46387	3.56	3071.86816	−0.07		
$R(3)$	3100.40161	−0.43	3076.30542	−0.14	3076.35669	0.43	3074.73560	1.80	3001.53974	−0.26
$R(4)$	3103.25952	1.17	3079.16797	0.75	3079.23096	1.84	3077.57568	−1.08	3004.38578	0.05
$R(5)$	3106.08789	−2.84	3082.00659	0.27	3082.08008	1.23	3080.39551	−1.54	3007.21063	0.48
$R(6)$	3108.89893	−0.18	3084.82324	0.44	3084.90576	0.40	3083.18970	−4.91	3010.01379	0.59
$R(7)$	3111.68286	−0.58	3087.61694	0.34	3087.70874	0.15	3085.96729	−2.08	3012.79490	0.05
$R(8)$	3114.44263	−1.02	3090.38818	0.52	3090.48926	0.77	3088.72241	1.14	3015.55429	−0.74
$R(9)$	3117.17871	−0.97	3093.13330	−2.61	3093.24219	−2.78	3091.45435	4.11	3018.29323	−0.48
$R(10)$	3119.89014	−1.33	3095.86157	0.28	3095.97705	−0.94	3094.15576	−0.48	3021.01218	1.35
$R(11)$	3122.58545	6.49	3098.56494	1.19	3098.68774	0.26	3096.83691	−2.28	3023.70685	0.49
$R(12)$	3125.24194	−0.15	3101.24023	−2.99	3101.37305	−0.32	3099.49951	0.47	3026.37988	−0.38
$R(13)$	3127.88110	0.30	3103.89990	0.25	3104.03467	−0.92	3102.13770	1.97	3029.03227	−0.22
$R(14)$	3130.49609	1.06	3106.53247	−0.51	3106.67505	0.95	3104.74805	−1.15	3031.66264	−0.36
$R(15)$	3133.08301	−1.72	3109.14233	−0.81	3109.28711	−1.71	3107.33911	−0.28	3034.27111	−0.67
$R(16)$	3135.64795	−1.89	3111.72974	−0.35	3111.87940	−0.30	3109.90552	−0.72	3036.85845	−0.33
$R(17)$	3138.19019	−0.11	3114.31421	20.45			3112.45044	0.74	3039.42369	−0.29
$R(18)$	3140.69849	−7.57	3116.83398	−0.12	3116.98926	−0.41	3114.96973	0.02	3041.96681	−0.54
$R(19)$	3143.19946	2.40	3119.35669	5.64	3119.50952	0.88	3117.46680	0.58	3044.48849	−0.38
$R(20)$	3145.66406	0.81	3121.84570	1.14	3122.00244	−1.09	3119.93701	−2.15	3046.98819	−0.32
$R(21)$	3148.10913	4.56					3122.39356	5.07	3049.46827	2.03
$R(22)$							3124.82813	13.98	3051.92201	−0.06
$R(23)$									3054.35542	−0.53
$R(24)$							3129.59302	−1.22	3056.76791	0.02
$R(25)$							3131.94678	−1.79	3059.15908	1.21
$R(26)$									3061.52550	−0.37
$R(27)$									3063.87227	0.38
$R(28)$										
$R(29)$									3068.49728	−0.70

dx.doi.org/10.1021/jp312879f | J. Phys. Chem. A 2013, 117, 9899−9907

Table 3. Observed Lines of HCO^+ in cm^{-1}

	12^00-02^00		12^20-02^20e		12^20-02^20f		11^11-01^11e		11^11-01^11f		10^02-00^02	
	ν	o−c × 10^3	ν	o−c × 10^3	ν	o−c × 10^3	ν	o−c × 10^3	ν	o−c × 10^3	ν	o−c × 10^3
$P(12)$	3003.56104	−0.37	3003.07031	−0.51	3003.09668	−0.62	3002.32007	−2.94			3001.56738	−0.50
$P(11)$	3006.77026	−0.07	3006.27588	0.03	3006.29590	0.06	3005.53174	−0.21	3005.51294	−0.35	3004.72998	−0.26
$P(10)$	3009.96069	0.72	3009.46021	−0.42	3009.47656	1.22	3008.71826	0.40	3008.68774	0.11	3007.87256	0.20
$P(9)$	3013.12964	−0.48		3018.89600	−0.59		3011.88086	0.17	3011.84180	0.24	3010.99634	2.18
$P(8)$	3016.28125	0.67		3022.00098	0.77		3015.02222	1.81	3014.97656	1.52	3014.09546	−0.10
$P(7)$	3019.41138	0.22		3025.08423	0.05		3018.13672	−0.24	3018.08765	−0.36	3017.17725	0.76
$P(6)$	3022.52173	0.05		3028.14844	−0.07		3021.22998	−0.32	3021.18042	0.00	3020.23657	−0.31
$P(5)$	3025.61279	0.84		3031.19312	−0.05		3024.30078	0.40	3024.25220	−0.02	3023.27661	−0.03
$P(4)$	3028.68140	−0.41					3027.34692	−0.22			3026.29614	0.42
$P(3)$							3030.37061	0.08	3030.33081	−2.91	3029.29395	−0.09
$P(2)$	3034.75952	−0.10					3033.37061	0.13	3033.34180	−1.51	3032.27148	−0.05
$P(1)$	3037.76758	0.33									3035.22730	−0.82
$R(0)$	3043.71875	−0.48									3041.07739	−0.95
$R(1)$	3046.66309	−0.20					3045.13550	0.84	3045.17285	0.49	3043.97192	0.08
$R(2)$	3049.58594	0.07		3049.04639	−0.44		3048.01660	0.13	3048.07715	0.20	3046.84546	1.29
$R(3)$	3052.48657	−0.27		3051.95288	−0.21		3050.87451	0.09	3050.96045	0.12	3049.69458	−0.70
$R(4)$	3055.36572	−0.36		3054.83936	−0.06		3053.70825	−0.21	3053.82227	−0.16	3052.52466	−0.45
$R(5)$	3058.22363	0.16		3057.70606	0.27		3056.51636	−2.14	3056.66284	−0.31	3055.33350	−0.08
$R(6)$	3061.05884	−0.05		3060.55200	−0.14		3059.30493	0.48	3059.48193	−0.49	3058.12061	−0.04
$R(7)$	3063.87231	0.07		3063.37891	0.51		3062.06616	−0.08	3062.28027	0.11	3060.88599	−0.26
$R(8)$	3066.66309	−0.33		3066.18457	0.06		3064.80420	0.43	3065.05640	0.11	3063.63843	8.11
$R(9)$	3069.43237	0.00		3068.96484	−5.55		3067.51660	−0.35	3067.81006	−0.65	3066.35254	−0.27
$R(10)$	3072.17896	−0.04					3070.20532	−0.38			3069.05371	0.04
$R(11)$	3074.90405	0.77	3074.48950	0.64	3074.47388	0.42	3072.86841	−1.50	3073.25513	1.04	3071.73218	−0.65
$R(12)$	3077.60498	−0.20	3077.21655	1.35	3077.19775	1.27	3075.51001	0.51	3075.94238	−0.49	3074.39014	−0.10
$R(13)$	3080.28418	−0.50	3079.92065	−0.38	3079.89575	−3.04	3078.12549	1.14	3078.61035	0.77	3077.02539	−0.47
$R(14)$	3082.94067	−1.13	3082.60645	0.29	3082.58057	0.25	3080.71436	−0.01	3081.25415	0.03	3079.63623	−3.40
$R(15)$	3085.57690	0.31	3085.27197	1.59	3085.24023	−0.75	3083.27710	−2.35	3083.87842	2.03	3082.22998	−1.51
$R(16)$	3088.18994	0.83	3087.91553	2.06	3087.88159	0.89	3085.81836	−1.12	3086.48071	4.41	3084.80054	−0.87
$R(17)$	3090.77881	−0.65	3090.58789	52.74	3090.54004	40.64	3088.33545	1.09	3089.05835	4.61	3087.34790	−1.43
$R(18)$	3093.34741	−0.34					3090.82568	1.71	3091.60230	−6.30	3089.87231	−2.89
$R(19)$									3094.10547	−35.32	3092.37915	0.17
$R(20)$	3098.41895	0.19									3094.86572	5.10
$R(21)$	3100.92261	0.77									3097.30981	−10.27
$R(22)$											3099.74829	−9.02
$R(23)$											3102.18701	14.73

dx.doi.org/10.1021/jp312879f | J. Phys. Chem. A 2013, 117, 9899−9907

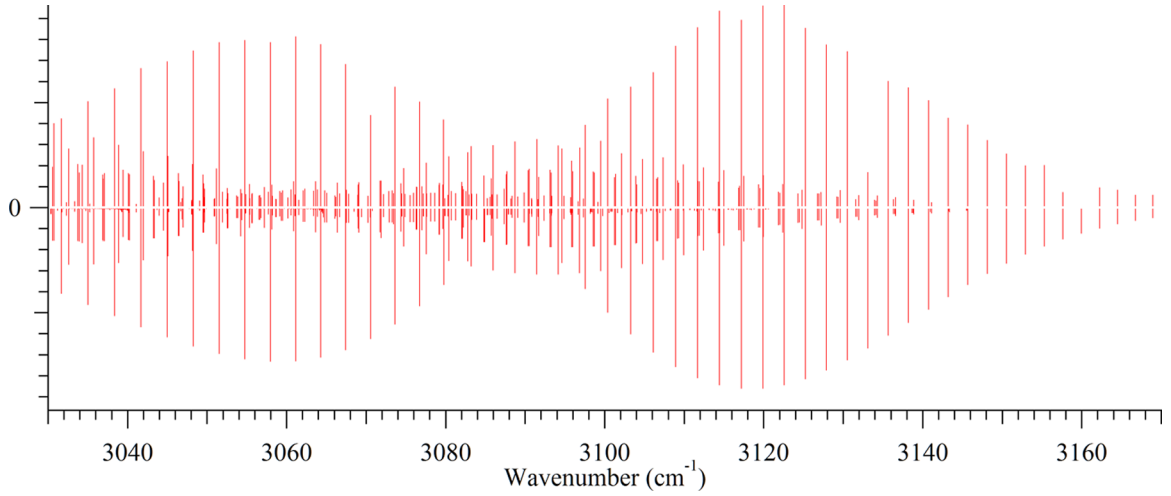

Figure 3. Stick spectrum of HCO^+ produced in a $He/H_2/CO$ plasma. The observed spectrum is displayed on the positive ordinate axis. The spectrum on the negative ordinate axis is calculated using the following temperatures: T_{rot} = 434 ± 7 K, T_1 = 3300 ± 240 K, T_2 = 841 ± 15 K, and T_3 = 3157 ± 68 K.

$$G_v = \sum_i \omega_i u_i + \sum_{i\le j} x_{ij} u_i u_j + \sum_{i\le j\le k} y_{ijk} u_i u_j u_k + l^2\left(g_e + \sum_i g_i u_i\right) \quad (2)$$

$$B_v = B_e - \sum_i \alpha_i u_i + \sum_{i\le j} \gamma_{ij} u_i u_j + \sum_{i\le j\le k} \gamma_{ijk} u_i u_j u_k + l^2\left(b_e + \sum_i b_i u_i\right) \quad (3)$$

$$D_v = D_e - \sum_i \beta_i u_i \quad (4)$$

with $u_i = v_i + 1/2$ for a stretching mode and $u_i = v_i + 1$ for the bending mode. The off-diagonal matrix elements that lead to the l-type doubling and resonance are

$$\langle v_2^l | H | v_2^{l\pm 2}\rangle = \frac{1}{4} q_v \sqrt{(v_2 \mp l)(v_2 \pm l + 2)} \times \sqrt{(J(J+1) - l(l\pm 1))(J(J+1) - (l\pm 1)(l\pm 2))} \quad (5)$$

with

$$q_v = q_e + \sum_i q_i u_i + \sum_{i\le j} q_{ij} u_i u_j \quad (6)$$

The infrared bands presented here were recorded prior to the microwave spectroscopy of Hirao et al.[19] Their work has led us to reconsider the fitting strategy we employ for our infrared data. Our original fits as referenced by Hirao et al. are available.[65] In particular, Hirao et al. note a difficulty in reconciling the value of g_e calculated using the photoionization data with the observed l-doubling in the 02^20 state. Using a value for q_v that is interpolated from the 01^10 and 03^10 states yields $g_e \approx 5.5$ cm^{-1}, which is considerably larger than the value predicted by the photoionization data, $g_e \approx 3.3$ cm^{-1}. Hirao et al. suggest that the 02^20 $J = 3$ term of Mayer et al.,[31] is perhaps instead due to $J = 2$. Unfortunately, Mayer et al. also report terms for 02^20 $J = 4$ and $J = 5$ that cannot be correct if the J assignments for the 02^20 state are all decreased by one.

In addition, inclusion of the photoionization data in our original fit led to values for x_{22} and y_{222} that are too large in magnitude, as these parameters adjusted to fit the 02^00 and 03^10 photoionization data from refs 31 and 32. This effect can be controlled by adding the data for 040−070 from ref 34 to the fit. However, we have chosen to constrain x_{22} to the value calculated by Prentice[34] and not include any photoionization data directly in our fit.

Finally, Hirao et al. note that there is considerable evidence of perturbations shifting the rotational constants of the higher vibrational states. Thus for the fit presented here, we have chosen to globally fit for the individual constants in the expansion of G_v but have not expanded B_v, D_v, and q_v. We have also chosen to implement our current fit using SPFIT,[66] so that the results can be more easily used by the community at large.

The results of our fit are presented in Table 1. This fit includes all of the rotational and rovibrational data to date. Our observed IR lines and the fit residuals are presented in Tables 2 and 3. The data files for the fit are provided as Supporting Information.

Rotational and Vibrational Temperatures. The relative intensity of each line is calculated assuming independent temperatures for rotation and each vibrational degree of freedom. The intensity I of a line is

$$I \propto S(J',l';J'',l'')\left(\frac{N''}{g''} - \frac{N'}{g'}\right) \quad (7)$$

where $S(J',l';J'',l'')$ is a Hönl−London line strength factor, N' and N'' are the number of molecules in the upper and lower states, and g' and g'' are the degeneracies of the upper and lower states. These number densities are

$$N = \frac{g}{Q}\exp\left(-\frac{hc}{k}\left(\frac{E - G_v}{T_{rot}} + \sum_i \frac{\omega_i v_i}{T_i}\right)\right) \quad (8)$$

where E is energy of the rovibrational state, Q is the partition function, T_{rot} is the rotational temperature, and T_i is the vibrational temperature of mode i.

The temperatures are calculated using a weighted least-squares regression of the observed line intensities. The weights for this regression are the uncertainties from line measurement;

dx.doi.org/10.1021/jp312879f | J. Phys. Chem. A 2013, 117, 9899−9907

i.e., the signal-to-noise ratio determines the weight of a line in the fit. However, there are a variety of experimental sources of error (such as variations in pressure and plasma current) that do not affect the signal-to-noise of a single measurement of a line but do affect the intensity uncertainty of the spectrum as a whole. Thus, the observed signal-to-noise ratio underestimates the uncertainty in the intensity. To correct for this, we multiply the uncertainties by a constant factor such that χ^2_{red} (χ^2 divided by the number of degrees of freedom in the fit) is one.

For the He-dominated plasma the temperatures were T_{rot} = 434 ± 7 K, T_1 = 3300 ± 240 K, T_2 = 841 ± 15 K, and T_3 = 3157 ± 68 K. The calculated and observed spectra from this scan are compared in Figure 3.

CONCLUSION

Knowledge of the hot bands and rotational constants of HCO^+ has been considerably increased by the measurements reported in this work. The global fit that we have made, including all previously published rotational and rovibrational spectra, provides the best determined set of molecular constants for this molecule.

The only data fitted in this work are rotationally resolved spectra of $H^{12}C^{16}O^+$. As referenced in the Introduction, there is also a wealth of data on other isotopologues. If scaling relationships between different isotopologues were used, or if a direct fit to a potential surface were made, then it would be possible to make a global fit of all isotopic data together, but this has not been attempted in the present work.

ASSOCIATED CONTENT

Supporting Information

SPFIT input and output files for the fit in Table 1. This material is available free of charge via the Internet at http://pubs.acs.org/.

AUTHOR INFORMATION

Corresponding Author

*E-mail: C.F.N., cfneese@physics.osu.edu; T.O., tozz@uchicago.edu.

Present Address

[‖]Department of Physics, The Ohio State University, Columbus, OH 43210, USA.

Notes

The authors declare no competing financial interest.

ACKNOWLEDGMENTS

P.S.K. is grateful to the University of Newcastle upon Tyne for a research studentship and to his advisor Iain R. McNab. This work has been supported by NSF grant PHY 03-54200.

REFERENCES

(1) Buhl, D.; Snyder, L. E. Unidentified Interstellar Microwave Line. *Nature* **1970**, *228*, 267−267.

(2) Klemperer, W. Carrier of the Interstellar 89.190 GHz Line. *Nature* **1970**, *227*, 1230−1230.

(3) Woods, R. C.; Dixon, T. A.; Saykally, R. J.; Szanto, P. G. Laboratory Microwave Spectrum of HCO^+. *Phys. Rev. Lett.* **1975**, *35*, 1269−1269.

(4) Herzberg, G. Spectra and Structures of Molecular Ions. *Q. Rev. Chem. Soc.* **1971**, *25*, 201−222.

(5) Douglas, A. E.; Herzberg, G. CH^+ in Interstellar Space and in the Laboratory. *Astrophys. J.* **1941**, *94*, 381−381.

(6) Herbst, E.; Klemperer, W. The Formation and Depletion of Molecules in Dense Interstellar Clouds. *Astrophys. J.* **1973**, *185*, 505−534.

(7) Watson, W. D. Ion−Molecule Reactions, Molecule Formation, and Hydrogen-Isotope Exchange in Dense Interstellar Clouds. *Astrophys. J.* **1974**, *188*, 35−42.

(8) Oka, T. In *Encyclopedia of Mass Spectrometry*; Armentrout, P. B., Ed.; Elsevier: Amsterdam, 2003; Vol. *1*; pp 217−226.

(9) Anicich, V. G.; Huntress, J., W. T. A Survey of Bimolecular Ion−Molecule Reactions for Use in Modeling the Chemistry of Planetary Atmospheres, Cometary Comae, and Interstellar Clouds. *Astrophys. J., Suppl. Ser.* **1986**, *62*, 553−672.

(10) Florescu-Mitchell, A. I.; Mitchell, J. B. A. Dissociative Recombination. *Phys. Rep.* **2006**, *430*, 277−374.

(11) Bogey, M.; Demuynck, C.; Destombes, J. L. Centrifugal Distortion Effects in HCO^+ from Its Millimetre Spectrum. *Mol. Phys.* **1981**, *43*, 1043−1050.

(12) Sastry, K. V. L. N.; Herbst, E.; De Lucia, F. C. Millimeter and Submillimeter Spectra of HCO^+ and DCO^+. *J. Chem. Phys.* **1981**, *75*, 4169−4170.

(13) Woods, R. C.; Saykally, R. J.; Anderson, T. G.; Dixon, T. A.; Szanto, P. G. The Molecular Structure of HCO^+ by the Microwave Substitution Method. *J. Chem. Phys.* **1981**, *75*, 4256−4260.

(14) Van den Heuvel, F. C.; Dymanus, A. Observation of Far-infrared Transitions of HCO^+, CO^+, and HN_2^+. *Chem. Phys. Lett.* **1982**, *92*, 219−222.

(15) Woods, R. C. Microwave Spectroscopy of Molecular Ions. *J. Mol. Struct.* **1983**, *97*, 195−202.

(16) Blake, G. A.; Laughlin, K. B.; Cohen, R. C.; Busarow, K. L.; Saykally, R. J. Laboratory Measurement of the Pure Rotational Spectrum of Vibrationally Excited $HCO^+(\nu_2 = 1)$ by Far-infrared Laser Sideband Spectroscopy. *Astrophys. J.* **1987**, *316*, L45−L48.

(17) Hirota, E.; Endo, Y. Microwave Spectroscopy of HCO^+ and DCO^+ in Excited Vibrational States. *J. Mol. Spectrosc.* **1988**, *127*, 527−534.

(18) Warner, H. E. The Microwave Spectroscopy of Ions and Other Transient Species in DC Glow and Extended Negative Glow Discharges. *Ph.D. Thesis*, The University of Wisconsin—Madison, 1988.

(19) Hirao, T.; Yu, S.; Amano, T. Submillimeter-wave Spectroscopy of HCO^+ in the Excited Vibrational States. *J. Mol. Spectrosc.* **2008**, *248*, 26−40.

(20) Gudeman, C. S.; Begemann, M. H.; Pfaff, J.; Saykally, R. J. Velocity-Modulated Infrared Laser Spectroscopy of Molecular Ions: the ν_1 Band of HCO^+. *Phys. Rev. Lett.* **1983**, *50*, 727−731.

(21) Amano, T. The ν_1 Fundamental Band of HCO^+ by Difference Frequency Laser Spectroscopy. *J. Chem. Phys.* **1983**, *79*, 3595−3595.

(22) Davies, P. B.; Rothwell, W. J. Diode Laser Detection of the Bending Mode of HCO^+. *J. Chem. Phys.* **1984**, *81*, 5239−5240.

(23) Kawaguchi, K.; Yamada, C.; Saito, S.; Hirota, E. Magnetic Field Modulated Infrared Laser Spectroscopy of Molecular Ions: The ν_2 Band of HCO^+. *J. Chem. Phys.* **1985**, *82*, 1750−1755.

(24) Foster, S. C.; McKellar, A. R. W.; Sears, T. J. Observation of the ν_3 Fundamental Band of HCO^+. *J. Chem. Phys.* **1984**, *81*, 578−579.

(25) Davies, P. B.; Hamilton, P. A.; Rothwell, W. J. Infrared Laser Spectroscopy of the ν_3 Fundamental of HCO^+. *J. Chem. Phys.* **1984**, *81*, 1598−1599.

(26) Liu, D. J.; Lee, S. T.; Oka, T. The ν_3 Fundamental Band of $HCNH^+$ and the $2\nu_3 \leftarrow \nu_3$ and $\nu_2 + \nu_3 \leftarrow \nu_2$ Hot Bands of HCO^+. *J. Mol. Spectrosc.* **1988**, *128*, 236−249.

(27) Keim, E. R.; Polak, M. L.; Owrutsky, J. C.; Coe, J. V.; Saykally, R. J. Absolute Infrared Vibrational Band Intensities of Molecular Ions Determined by Direct Laser Absorption Spectroscopy in Fast Ion Beams. *J. Chem. Phys.* **1990**, *93*, 3111−3119.

(28) Dyke, J. M.; Jonathan, N. B. H.; Morris, A.; Winter, M. J. The First Ionization Potential of the Formyl Radical, $HCO(X^2A')$, Studied Using Photoelectron Spectroscopy. *Mol. Phys.* **1980**, *39*, 629−636.

(29) Dyke, J. M. Properties of Gas-phase Ions. Information to be Obtained from Photoelectron Spectroscopy of Unstable Molecules. *Faraday Trans. 2* **1987**, *83*, 69−87.
(30) Mayer, E.; Grant, E. R. Double-Resonance Spectroscopy of the High Rydberg States of HCO. I. A Precise Determination of the Adiabatic Ionization Potential. *J. Chem. Phys.* **1995**, *103*, 10513−10519.
(31) Mayer, E. E.; Hedderich, H. G.; Grant, E. R. Double-Resonance Spectroscopy of the High Rydberg States of HCO. III. Multiple Pathways in the Vibrational Autoionization of the Bending Overtone. *J. Chem. Phys.* **1998**, *108*, 8429−8435.
(32) Foltynowicz, R. J.; Robinson, J. D.; Zuckerman, E. J.; Hedderich, H. G.; Grant, E. R. Experimental Characterization of the Higher Vibrationally Excited States of HCO^+: Determination of ω_2, x_{22}, g_{22}, and B(030). *J. Mol. Spectrosc.* **2000**, *199*, 147−157.
(33) Zuckerman, E. J.; Mayer, E. E.; Foltynowicz, R. J.; Robinson, J. D.; Jen, S. H.; Konopka, M. C.; Sanford, T.; Hedderich, H. G.; Chen, I. C.; Grant, E. R. Double-Resonance Spectroscopy of the High Rydberg States of HCO. V. Rovibronic Interactions and *l*-Uncoupling in the (010) Manifold. *J. Chem. Phys.* **2000**, *113*, 5372−5383.
(34) Prentice, K. The Rydberg Spectroscopy of the HCO Radical and the Spectroscopic Characterization of the Vibrational Force Field of HCO^+. *Ph.D. Thesis*, Purdue University, 2005.
(35) Foster, S. C.; McKellar, A. R. W. The ν_3 Fundamental Bands of HN_2^+, $DN2^+$, and DCO^+. *J. Chem. Phys.* **1984**, *81*, 3424−3428.
(36) Kawaguchi, K.; McKellar, A. R. W.; Hirota, E. Magnetic Field Modulated Infrared Laser Spectroscopy of Molecular Ions: The ν_1 Band of DCO^+. *J. Chem. Phys.* **1986**, *84*, 1146−1148.
(37) Dore, L.; Cazzoli, G. Investigation of a Vibration-Rotation Interaction in DCO^+ by Millimeter Wave Spectroscopy. *Chem. Phys. Lett.* **1996**, *257*, 460−464.
(38) Dore, L.; Beninati, S.; Puzzarini, C.; Cazzoli, G. Study of Vibrational Interactions in DCO^+ by Millimeter-wave Spectroscopy and Determination of the Equilibrium Structure of the Formyl Ion. *J. Chem. Phys.* **2003**, *118*, 7857−7862.
(39) Hirao, T.; Yu, S.; Amano, T. Submillimeter-wave Spectroscopy of DCO^+ in the Excited Vibrational States: Does the Stark Effect Cause Anomalies in the (02^20) State? *J. Chem. Phys.* **2007**, *127*, 074301/1−12.
(40) Plummer, G. M.; Herbst, E.; Delucia, F. C. Laboratory Measurement of the $J = 2 \rightarrow 3$ Rotational Transition Frequency of $HC^{17}O^+$. *Astrophys. J.* **1983**, *270*, L99−L100.
(41) Dore, L.; Cazzoli, G.; Caselli, P. Laboratory and Astrophysical Detection of the Hyperfine Structure of the $J = 1−0$ Rotational Transition of $HC^{17}O^+$. *Astron. Astrophys.* **2001**, *368*, 712−715.
(42) Snyder, L. E.; Hollis, J. M.; Lovas, F. J.; Ulich, B. L. Detection, identification, and observations of interstellar $H^{13}CO^+$. *Astrophys. J.* **1976**, *209*, 67−74.
(43) Hollis, J. M.; Snyder, L. E.; Lovas, F. J.; Buhl, D. Radio detection of interstellar DCO^+. *Astrophys. J.* **1976**, *209*, L83−L85.
(44) Dore, L.; Puzzarini, C.; Cazzoli, G. Millimetre-wave Spectrum of $HC^{17}O^+$. Experimental and Theoretical Determination of the Quadrupole Coupling Constant of the ^{17}O Nucleus. *Can. J. Phys.* **2001**, *79*, 359−366.
(45) Guelin, M.; Thaddeus, P. Detection of $HC^{18}O^+$ in Sagittarius B2. *Astrophys. J.* **1979**, *227*, L139−L141.
(46) Guelin, M.; Cernicharo, J.; Linke, R. A. Detection of $HC^{17}O^+$ in Sagittarius B2. *Astrophys. J.* **1982**, *263*, L89−L93.
(47) Brown, J. In *Polyatomic Radicals and Ions*; Hüttner, W., Ed.; Landolt-Börnstein - New Series; Springer-Verlag: Berlin, 1995; Vol. *II/19d2*, pp 302−309.
(48) Guelachvili, G.; Rao, K. N. In *Linear Triatomic Molecules*; Guelachvili, G., Ed.; Landolt-Börnstein - New Series; Springer-Verlag, 1995; Vol. *II/20b1*; pp 198−201.
(49) Bjorklund, G. C. Frequency-Modulation Spectroscopy - New Method for Measuring Weak Absorptions and Dispersions. *Opt. Lett.* **1980**, *5*, 15−17.
(50) Wang, R.; Chen, Y.; Cai, P.; Lu, J.; Bi, Z.; Yang, X.; Ma, L. Optical Heterodyne Velocity Modulation Spectroscopy Enhanced by a Magnetic Rotation Effect. *Chem. Phys. Lett.* **1999**, *307*, 339−342.
(51) Luo, M.; Bi, Z.; Cai, P.; Wang, R.; Yang, X.; Chen, Y.; Ma, L. Optical Heterodyne Magnetic Rotation Enhanced Velocity Modulation Spectroscopy: A Sensitive Absorption-based Scheme for Paramagnetic Molecular Ions. *Rev. Sci. Instrum.* **2001**, *72*, 2691−2696.
(52) Tarsitano, C. G.; Neese, C. F.; Oka, T. High-Resolution Spectroscopy of the $2^2\Pi_u \leftarrow X^4 \sum_g^-$ Forbidden Transistions of C_2^+. *J. Chem. Phys.* **2004**, *121*, 6290−6297.
(53) Gottfried, J. L.; McCall, B. J.; Oka, T. Near-infrared Spectroscopy of H_3^+ above the Barrier to Linearity. *J. Chem. Phys.* **2003**, *118*, 10890−10899.
(54) Gottfried, J. L.; Oka, T. Near-infrared Electronic Spectrum of CH_2^+. *J. Chem. Phys.* **2004**, *121*, 11527−11529.
(55) Lindsay, C. M.; Rade, R. M.; Oka, T. Survey of H_3^+ Transitions between 3000 and 4200 cm^{-1}. *J. Mol. Spectrosc.* **2001**, *210*, 51−59.
(56) Pate, B. H.; Lehmann, K. K.; Scoles, G. The Onset of Intramolecular Vibrational Energy Redistribution and Its Intermediate Case: The ν_1 and $2\nu_1$ Molecular Beam, Optothermal Spectra of Trifluoropropyne. *J. Chem. Phys.* **1991**, *95*, 3891−3916.
(57) Pine, A. S. Tunable laser survey of molecular air pollutants. Final Report NSF/ASRA/DAR 78-24562, MIT: Lexington, MA, 1980. http://www.ntis.gov/search/product.aspx?ABBR=PB80180003.
(58) Rothman, L. S.; Barbe, A.; Chris Benner, D.; Brown, L. R.; Camy-Peyret, C.; Carleer, M. R.; Chance, K.; Clerbaux, C.; Dana, V.; Devi, V. M. The HITRAN Molecular Spectroscopic Database: Edition of 2000 Including Updates through 2001. *J. Quant. Spectrosc. Radiat. Transfer* **2003**, *82*, 5−44.
(59) Rothman, L. S.; Jacquemart, D.; Barbe, A.; Chris Benner, D.; Birk, M.; Brown, L. R.; Carleer, M. R.; Chackerian, J. C.; Chance, K. The HITRAN 2004 Molecular Spectroscopic Database. *J. Quant. Spectrosc. Radiat. Transfer* **2005**, *96*, 139−204.
(60) Stephenson, S. K.; Saykally, R. J. Velocity Modulation Spectroscopy of Ions. *Chem. Rev.* **2005**, *105*, 3220−3234.
(61) Oka, T. In *Frontiers of Laser Spectroscopy of Gases*; Alves, A. C. P., Brown, J. M., Hollas, J. M., Eds.; Kluwer Academic: Norwell, MA, 1988; Vol. *234*; pp 353−377.
(62) Kabbadj, Y.; Huet, T. R.; Rehfuss, B. D.; Gabrys, C. M.; Oka, T. Infrared Spectroscopy of Highly Excited Vibrational Levels of Protonated Nitrogen, HN_2^+. *J. Mol. Spectrosc.* **1994**, *163*, 180−205.
(63) Brown, J. M.; Hougen, J. T.; Huber, K. P.; Johns, J. W. C.; Kopp, I.; Lefebvre-Brion, H.; Merer, A. J.; Ramsay, D. A.; Rostas, J.; Zare, R. N. The Labeling of Parity Doublet Levels in Linear Molecules. *J. Mol. Spectrosc.* **1975**, *55*, 500−503.
(64) Winnewisser, M.; Winnewisser, B. P. Millimeter Wave Rotational Spectrum of HCNO in Vibrationally Excited States. *J. Mol. Spectrosc.* **1972**, *41*, 143−176.
(65) Neese, C. F. Laser Spectroscopy of Molecular Cations of Astrophysical Interest. *Ph.D. Thesis*, The University of Chicago, 2012.
(66) Pickett, H. M. The Fitting and Prediction of Vibration-Rotation Spectra with Spin Interactions. *J. Mol. Spectrosc.* **1991**, *148*, 371−377.